

Cell Protrusions

George Oster

Departments of Molecular and Cellular Biology and Entomology
University of California, Berkeley, CA 94720

Alan S. Perelson

Theoretical Division
Los Alamos National Laboratory
Los Alamos, NM 87545

Introduction

How do cells move? There is no shortage of theories, but a definitive answer is still elusive. Here we will present some models for cell motions along with proposals for experiments to address the theories. We will restrict ourselves to the problem of cell protrusion, although the models apply to other motility phenomena as well.

Different protrusion phenomena extend at different characteristic rates. Figure 1 shows data for protrusion rates of lamellipodia, filopodia and the acrosomal process of *Thyone*. Their velocities vary dramatically, which suggests that the force driving them may originate from different physical mechanisms. We will present here models for each of these processes.

Lamellipod protrusion

Lamellipodia are broad, flat cytoplasmic protrusions that spread out in front of a moving cell. Experiments have shown that there is surface flow of cytoplasm rearward from the leading edge as the lamellipodium extends forward [20]. Conservation of mass ensures that there must be a central flow of cytoplasm forward to provide the material for extension. The question we address is: what forces drive the extension of the leading lamella? Amoebae pseudopodia bear superficial resemblance to lamellipodia, but there is evidence that they may operate by a different mechanism, and so we will not deal with them here;

models of the “frontal contraction” and “cortical tractor” hypotheses for amoeboid motion can be found in [16, 17, 25, 26, 27].

An elegant set of models have been developed by Dembo, Alt, and their coworkers based on the idea that cytoplasm can be modeled as a “contractile fluid” [1, 7, 8, 9]. They model the cytogel as a two-phase, viscous fluid (i.e. a Navier-Stokes system) with a term added that permits the gel phase to contract, then disassemble. Their numerical simulations show that such a fluid can indeed drive cytoplasmic flows in ways that appear realistic. Their model assumes the force driving the fluid phase derives from myosin-driven sliding of (counter-oriented) actin fibers and that neither cytoskeletal elasticity nor osmotic pressure play an important role. The contraction of the actin phase creates hydrostatic pressure gradients that impel the cytoplasm forward. While this model has much to recommend it, there are two experiments that cause some difficulty. First, scanning microscopy of the leading lamella reveals an apparently random, anastomosing network of actin fibers, rather than a fluid of shorter and/or counter-oriented filaments that could support myosin driven contraction [14, 15]. Second, opening fluid channels to the extracellular environment should dissipate most of the cell’s internal hydrostatic pressure; however, permeabilizing the cell does not inhibit protrusive activity [5, 18]. Neither of these observations are necessarily fatal since many artifacts arise in preparing a cell for scanning electron microscopy, and the hydrodynamic resistance of the membrane fluid channels may still support some internal hydrostatic pressure. Nevertheless, we have taken a different view of lamellipodial protrusion. In addition to the above experiments, we were captured by the early observation that raising a cell’s osmotic environment generally arrested lamellipodial protrusion—although it enhanced other protrusive activity, as we shall discuss below [47]. Thus our attention was drawn to the role of elastic and osmotic forces in driving cell protrusion.

The solution-expansion model

The basic idea underlying the solution-expansion (SE) model is that gel osmotic pressure drives lamellipodial protrusion [28, 29, 30, 31, 32]. The cortical actin gel, like other polyelectrolyte gels, is in mechanical equilibrium when its osmotic pressure is just balanced by its elastic stress. The osmotic pressure arises from the entropic motions of the chains and their counterion pressure: positive counterions to the gel’s fixed negative charges cannot escape the from the gel because of the constraint of electroneutrality (c.f. Appendix A).

Thus the counterions can be viewed as a gas contained within the boundaries of the gel. Resisting this pressure are the elastic tensions in the gel's fibers. At mechanical equilibrium, these opposing forces just balance one another, as shown in Figure 2a. The elastic modulus of a gel, E , is proportional to the number of crosslinked chains, ρ : $E \propto \rho$ [24]. Therefore, if the gel solates, i.e. some of actin filaments are severed, the elastic modulus of the gel is reduced and the gel swells to a new equilibrium. The swelling of an electrically neutral gel is driven only by the entropic motions of the chains, and Tanaka and his coworkers have shown that its time course is as if the gel fibers are diffusing into the surrounding fluid with a diffusion coefficient $\hat{D} \propto \rho^{-1}$ [24, 44], and so the displacement of a neutral gel boundary follows $R(t) \propto \sqrt{t}$ where $R(t)$ is the gel radius. The swelling of a charged gel is more complicated, for the swelling dynamics are dominated by the ion pressure. The initial swelling rate is characterized by a time constant (τ, τ_{ion}) , where τ_{ion} is a function of the counterion concentration [12]. In general, ionic gels swell much faster than neutral gels, at least in their initial stages $R > \sqrt{t}$ [23]. In Appendix B we argue that the swelling of an ionic gel follows an equation of the form:

$$\frac{dR}{dt} = E(R_0 - R) + \frac{A}{R^n} \quad [1]$$

where τ is the frictional resistance the gel offers to the cytosol, A is a constant characterizing the ionic contribution to the gel osmotic pressure, and $n \geq 1$ depends on the geometry.

The scenario that emerges from the SE model shown in Figure 2. Activated cytosolic solation bind to, sever, and cap actin filaments. This weakens the gel and allows it to osmotically expand. Soon following expansion the gel commences to reanneal as actin filaments nucleate, elongate and cross-link. The initiating event can be either intra or extra cellular. For example, binding of a ligand to a receptor can trigger a rise in cytosolic calcium (e.g. via the inositol signaling pathway) that activates solating factors such as gelsolin [19, 41, 48]. The SE model predicts that a *microscopic* observation of the leading lamella should show that the leading edge moves forward *locally* faster than \sqrt{t} . However, the *macroscopic* movement of the lamella is the result of many local solation-expansion-gelation cycles, and so the overall motion may appear almost constant, $L \propto t$. Felder and Elson measured the velocity of lamellipodial extension in fibroblasts and found $0.07 < v < 0.12$ $\mu\text{m}/\text{sec}$. [11]. Since each cycle can only commence after regelation has completed, the

overall movement of the lamellipodia is limited by the rate of actin polymerization [42]. This points to the necessity of obtaining very fine-grained observations of lamellipodial extension to see if these predictions are borne out.

Filopod protrusion

Filopodia grow as long (3-5 μm), thin (50-100 nm) cellular protrusions containing an actin core that polymerizes at the tip of the extension. They extend much faster than lamellipodia, sometimes as fast as $dL/dt = 0.16 \mu\text{m}/\text{sec}$ [2]. Most strikingly, raising external osmolarity eventually causes lamellipodia to cease protruding, while filopodia actually protrude faster [4]. This together with the fact that the actin is organized into a parallel bundle, rather than a nearly isotropic gel suggests that they protrude by a quite different mechanism from lamellipodia. There is evidence that molecular motors may be involved in filopodial protrusion [40, 49]; however, a much simpler mechanism appears to explain many aspects of this phenomenon, which we called the “Brownian Ratchet” model (BR) [36].

Consider a single actin filament, polymerizing freely in solution. The velocity of the tip is given by $dL/dt = (\text{monomer size}) \cdot (\text{polymerization rate}) = \lambda \cdot (k_{\text{on}}M - k_{\text{off}}) = 2.5 \text{ nm} \cdot (11.3 / \text{sec} \cdot \mu\text{M} \cdot 25 \mu\text{M} - 1.4 / \text{sec}) = 0.7 \mu\text{m}/\text{sec}$, where λ is half the size of a monomer (since actin is a staggered double helix), M is the local actin concentration, and k_{on} and k_{off} are the polymerization and depolymerization rate constants at the barbed end [37]. Since measured filopodial velocities are about a fifth this large, something must be hindering free polymerization. Consider the situation shown in Figure 3a: the free polymerization is blocked by an object whose diffusion coefficient is D , so that a monomer can add to the tip only when the gap between the tip and the object is at least λ . If $k_{\text{off}} = 0$, and $k_{\text{on}} \gg 1$, then each time the object diffuses a distance beyond the tip, its motion will be “ratcheted” by the addition of a monomer. The time to diffuse a length λ is $T = \lambda^2/2D$. Then the time to diffuse a distance $L = N \cdot \lambda$ is simply $N \cdot T$:
 $T = N \cdot T = N \cdot \frac{\lambda^2}{2D} = L \frac{\lambda}{2D}$. The average velocity of the particle is $\langle v \rangle = L/T$, and so the average speed of a particle that is “ratcheted” at intervals λ is

$$\langle v \rangle = \frac{2D}{\lambda}. \quad [2a]$$

This is the speed of an ideal Brownian ratchet. If the motion of the diffusing object is biased by a load force, f , and if the polymerization is not instantaneous, it is possible to derive a relationship giving the velocity corresponding to any load (Appendix C; [36]). Figure 3b shows the velocity of the ratchet under any load. If the polymerization and depolymerization velocities are much slower than the ideal ratchet velocity, i.e. $k_{\text{on}}M \cdot \lambda, k_{\text{off}} \cdot \lambda \ll 2D/\lambda$, then the ratchet equation reduces to a startlingly simple formula:

$$v = \left[k_{\text{on}} M e^{-f \cdot \lambda / k_B T} - k_{\text{off}} \right] \cdot \lambda \quad [2b]$$

where $f \cdot \lambda / k_B T$ is the dimensionless work done against the load. That is, the polymerization rate, $k_{\text{on}} \cdot M$, is weighted by the probability that a thermal fluctuation of the load opens up a monomer-sized gap, λ . Here M is the concentration of actin monomers at the tip of the filopod. Note that in this limit the ratchet velocity does not depend on the diffusion coefficient of the load. Since filopodial velocities are much slower than the ideal ratchet velocity for an object of this size, the approximate formula [2b] is valid. The force required to stall the ratchet is found by setting $v = 0$ in the above expression, which yields the familiar equilibrium thermodynamic relationship $k_{\text{off}}/k_{\text{on}}M = \exp(f \cdot \lambda / k_B T)$, or

$$f_o = -\frac{k_B T}{\lambda} \ln \frac{k_{\text{off}}}{k_{\text{on}} M} \quad [2c]$$

which is valid for all parameter values. Now consider a filopod of radius 50 nm loaded only by a typical membrane tension of 0.035 dyne/cm [3, 10], so that the load is $f = 2 \cdot (50 \times 10^{-7} \text{ cm})(0.035 \text{ dyne/cm}) = 1.1 \times 10^{-6}$ dyne. Equation [2c] shows that a single actin filament could not extend against such a load. However, 20 filaments acting in parallel could easily move this load at the observed velocity ($v = 0.15 \mu\text{m/sec}$) with a monomer concentration of only $M = 8 \mu\text{M}$.

Eventually, as the filopod extends, diffusion of monomers down the filopod shaft will limit the monomer concentration at the tip, so that the protrusion rate is governed by the equations:

$$\frac{dL}{dt} = \underset{\text{Ratchet velocity}}{v(M)} \quad [3a]$$

$$\frac{dM}{dt} = \underbrace{\frac{D_M}{L} (M_o - M)}_{\text{diffusion supply to tip}} - n \underbrace{(k_{\text{on}} e^{-M} - k_{\text{off}})}_{\text{polymerization}} \quad [3b]$$

where M (μM) is the concentration of monomers at the filopod tip, M_o is the monomer concentration at the base, L_o is the initial length, D_M is the monomer diffusion coefficient, and n the concentration of tips (in μM)¹. For a filopod, the approximate equation (1b) is satisfactory. The numerical solution of these equations shown in Figure 3d displays the correct qualitative behavior: protrusion initially follows $L \propto t$ (constant velocity), until diffusion of monomers becomes limiting, whereupon the curve follows $L \propto \sqrt{t}$. Note that there is nothing in the model that limits the final length of the filopod. For that, we would have to include in the kinetics an additional effect, such as ‘dynamic instability’ [22, 43].

The free energy driving the BR mechanism derives from the free energy of actin polymerization, which far exceeds the $10^4 k_B T$ it takes to deform the plasma membrane from a plane into a filopod.² However, the transduction is indirect: the proximal *force* for move-

¹ To express n in μM we divide by the volume of the tip, $\text{Area} \times \text{height}$, then divide by 6×10^{14} to convert number/cm³ to μM .

² If we model a filopod as a cylinder with a hemispherical cap, then we can compute how much energy it takes to form such a structure from a planar bilayer. Using $B = 50 k_B T$, the energy required to bend a membrane into a hemispherical cap is $W = \int_0^{\pi/2} (B/2) (1/R^2) dA = 2 \pi B = 300 k_B T$. To create a membrane cylinder of radius 50 nm and $L = 1 \mu\text{m}$ costs $3000 k_B T / \mu\text{m}$. To elongate by 1 ratchet distance, $\delta = 2.5 \text{ nm}$, against a membrane tension of about $\sigma = 0.035 \text{ dyne/cm}$ —equivalent to a load force of 11 pN —costs $6.6 k_B T$, so that a protrusion of $5 \mu\text{m}$ requires $1.3 \times 10^4 k_B T$ of work. Thus the total work to create a filopod $5 \mu\text{m}$ long and 50 nm radius = $300 + 1.3 \times 10^4 + 3 \times 10^3 = 1.6 \times 10^4 k_B T$. The binding energy of an actin monomer is $-13.6 k_B T/\text{monomer}$, making the process $8/13.6 \sim 60\%$ efficient. Each monomer, before attaching to the filament, binds one ATP which is hydrolyzed sometime after the monomer attaches. Each hydrolysis yields about $\Delta G = -15-20 k_B T/\text{molec} = 62 \text{ pN-nm/ATP}$, if we were to add this to the ATP contribution we would have a total free energy drop of $\Delta G = -30 k_B T/\text{monomer}$. However, since ATP is hydrolyzed after polymerization its contribution to force generation is not important. The

ment arises from random thermal fluctuations of the *load*, while the chemical potential release accompanying polymerization acts to rectify the thermal motions of the load. The binding free energy of a monomer to the end of an actin filament must be tight enough to prevent the load from back diffusion. If G_b were $\sim k_B T$, the residence time of the monomer would be short and the site would likely be empty when the load experiences a reverse fluctuation—or, if the site is occupied, the force of its collision with the load would dislodge the monomer. Hence the concentration of monomers and the binding free energy of polymerization supply the free energy to implement the ratchet. Thus the BR process does not violate the Second Law; rather it borrows from the available thermal energy to drive the ratchet.

Sheetz and his coworkers found that extending filopodia can buckle if they contact the substratum [40]. This implies that there is an axial force generated by the filopod sufficient to buckle it, and so they inferred that filopodial protrusion could be driven by myosins. Myosin I is known to localize in the leading edge membrane and in filopodia [49]. Such a force would require several hundred myosin molecules.³ Using the formula for the stall load of a BR, we compute that the ratchet can also bend a filopod if the monomer concentration is greater than 20 M. Therefore, both proposed mechanisms can buckle a filopod and a mechanical calculation cannot distinguish between them.

viscous work against the fluid medium is inconsequential compared to the bending energy, so we can neglect it in this estimate.

³ We can estimate this force from the Euler buckling formula for thin rods: $F_{cr} = \pi^2 B/4L^2$, where B is the bending modulus = Young's modulus (E) \times moment of inertia (I) [21]. If we use for Young's modulus of a single actin filament $E = 2.5 \cdot 10^9 \text{ N/m}^2 = 2.5 \times 10^8 \text{ pN/nm}^2$, the buckling load for a single filament of length $L = 5 \text{ }\mu\text{m}$ and diameter = 10 nm is $1.9 \times 10^{-7} \text{ dyne} = 1.9 \text{ pN}$. If a myosin can exert an average force of 2 pN, then a single myosin could bend a filament of this length. If the filopod consists of a close-packed hexagonal array of actin fibers it will form a bundle of 38 actin filaments with a cylindrical of diameter $\sim 35 \text{ nm}$. Then ~ 360 myosins are required to buckle the filopod.

Can actin polymerization drive lamellipodial protrusion?

Several authors have proposed that lamellipodia are driven by actin polymerization [42]. The response of lamellipodia to hyperosmolarity argues against this: increasing the concentration of monomers by dehydrating the cortex should speed up polymerization, not arrest protrusion as is observed. Moreover, as our analysis of the BR demonstrates, polymerization can only produce an extension force by rectifying the diffusion of a load. In the case of lamella, it is not clear what this load is. Electron micrographs of the leading edge do not show any consistent orientation of the actin fibers; indeed most of the gel in the neighborhood of the membrane is organized circumferentially, with but a small percentage of filaments oriented normal to the membrane with the barbed end outwards. Nevertheless, it is possible that more detailed micrographs of the structure of the very leading edge may yet reveal the necessary polarized structures requisite for the BR mechanism.

***Listeria* and Inductopodia**

The bacterium *Listeria monocytogenes* moves through the cellular cytoplasm with velocities 0.05-1.5 $\mu\text{m}/\text{sec}$ [6, 39, 44, 46]. It moves trailing a long tail of polymerized actin consisting of many short filament crosslinked into a meshwork. Actin is inserted into the tail adjacent to the bacterium, and the average orientation of the fibers is with their barbed ends in the direction of motion. Several authors have suggested that the bacterium is driven forward by the oriented polymerization of the actin tail [39, 44]. since treatment with agents that disrupt actin polymerization stop movement, but poisons for myosin do not. A computation using equation [1] shows that the BR mechanism is consistent with the observed velocities.

A related phenomenon was reported by Forscher, et al. [13]. They found that positively charged polystyrene beads placed atop lamellipodia grow *Listeria*-like tails and move across the surface of the cell with velocities comparable with *Listeria*. We propose that these motions are another manifestation of the BR mechanism.

The acrosomal process in *Thyone*.

Tilney and Inoué used video microscopy to observe and measure the protrusion velocity of the acrosomal process in the sea cucumber *Thyone*. Their data showed that the length of the process increased as the square root of the time, or $L^2 \sim t$. Since $v \propto \sqrt{t}$ is characteristic of diffusion processes, they inferred that the protrusion was driven by the polymerization of the actin core, with diffusion of monomers from the acrosomal cup at the base of the protrusion being the limiting process. However, a calculation showed that diffusion could not supply monomers fast enough to the tip to keep up with the observed protrusion velocity, and so another mechanism must be involved. Oster and Perelson proposed that the protrusion was driven by hydrostatic pressure generated by the osmotic expansion of the acrosomal cup, which is packed almost solid with actin monomers complexed with profilin [32, 33, 35]. A calcium shock can trigger osmotic influx of water into the cup, and the resulting influx of water drives a large hydrostatic pressure head that propels the acrosomal process outward. The protrusion velocity driven by this pressure had the form

$$(L) \frac{dL}{dt} = p_{tip} - p_o \quad [4]$$

where $L(t)$ is the length of the acrosomal shaft, (L) is the viscous drag on the shaft, and p_o is proportional to the osmotic pressure in the cup. Since p_o should be nearly constant during most of the protrusion due to the high concentration of protein in the cup, and since the viscous drag on a cylinder increases as the shaft extends, $(L) \propto L$, the protrusion rate is $L \frac{dL}{dt} = \frac{dL^2}{dt} = \text{Constant}$, i.e. $L^2 \propto t$. Thus viscous limited motion driven by a constant force also follows a \sqrt{t} velocity dependence identical to diffusion.⁴ This interpretation was confirmed by Tilney and Inoué when they subjected the system to various external osmolarities

⁴ Actually, the friction coefficient of a cylinder is $(L) = 2 \mu L / [\ln(L/r) - 0.807]$, where μ is the fluid viscosity and r the cylinder radius. If we use this in equations [4] we find that the cylinder grows as $\text{Ei}[2 \cdot \ln(L)] \sim t$, where $\text{Ei}[z]$ is the exponential integral (i.e. $d/dt[\text{Ei}[2 \cdot \ln(L)]] = (L/\ln(L))dL/dt$). At long lengths this rises more slowly than L^2 ; i.e. on a log plot the slope is about 1.4 rather than 2. From Tilney and Inoué's data it is not easy to distinguish this difference. However, in principle, it could be used to distinguish between viscous-limited motion and strictly diffusion limited motion.

[45]. As expected, they found that hyperosmotic conditions slowed the protrusion rate, and hypo-osmotic conditions speeded it up. Figure 4 shows a fit of the hydrostatic model to the data of Tilney and Inoué.

A comparison of velocities of protrusion

Table 1 summarizes various aspects of the three protrusive organelles we have discussed. Providing sufficiently accurate measurements can be performed, one way of distinguishing between different mechanisms of protrusion is by their differing velocities.

	Lamellipodia & Blebs	Filopodia	Acrosome
Protrusion force	Gel osmotic pressure	Brownian ratchet	Hydrostatic pressure
Protrusion velocity	$v \approx 0.03\text{-}0.1 \mu\text{m}/\text{sec}$	$v \approx 0.16 \mu\text{m}/\text{s}$	$v \approx 15 \mu\text{m}/\text{sec}$
Initial protrusion rate	Lamellipod: $L > \sqrt{t}$ locally, but $L \propto t$ macroscopically Bleb: Volume = const. $\times t$	$L \propto t$	$L \propto \sqrt{t}$
Osmotic response of protrusion rate	Hypertonic slows	Hypertonic speeds up	Hypertonic slows
Effect of permeabilizing the plasma membrane	Protrusion still can occur	?	?

Table 1. Characteristics of protrusive processes.

Discussion

The chemical controls that regulate and direct cell movement are proving more intricate than anyone imagined. However, the issue of what drives cellular protrusion is finally a question of physics. We have presented several models of cellular protrusion. They do not by any means exhaust the possibilities; however, they do provide a framework within which

to understand the current experimental literature and to contemplate new experiments. In summary, we propose that (a) lamellipodia are driven by cycles of local solation, osmotic expansion and re-gelation. This produces an overall velocity that is constant and limited by the rate of actin polymerization at the very leading edge. (b) Filopodial and microvillus protrusion are driven by actin polymerization. However, the polymerization process itself exerts no force; rather polymerization rectifies the diffusive motion of the load upon which the polymer impinges. We call this phenomenon the Brownian Ratchet. The movement of the bacterium *Listeria monocytogenes* and the polymerization-induced motion exhibited by polyanionic beads placed on the cell surface both appear to be driven by the Brownian ratchet mechanism. There is good evidence that myosin also participates in filopodia protrusion, but probably not in *Listeria* or inductopodia propulsion. (c) The acrosomal process in the sea cucumber *Thyone* is driven by hydrostatic pressure generated by osmotic swelling of the acrosomal cup. The protrusion rate of each of these phenomena are described by a scaling law of the form $(\text{length}) \propto (\text{time})^q$ summarized in Table 1. Consistency with these predictions do not prove the proposed mechanism, for several different physical phenomena can have the same velocity scaling law. Nevertheless, the scaling laws may prove useful in discarding certain mechanisms. q

ACKNOWLEDGMENTS

GFO was supported by NSF Grant No. DMS-8618975. Portions of this work were performed under the auspices of the U. S. Department of Energy and the Neurosciences Institute. We would like to acknowledge our colleagues Charlie Peskin, Garry Odell, Jim Murray, and Paul Janmey, with whom these ideas were developed. Many of our experimental colleagues graciously shared their unpublished results with me which provided a salutary reality check on our theoretical work, especially, Paul Janmey, Casey Cunningham, John Hartwig, Tom Stossell, Manfred Schliwa, Lew Tilney, Tom Pollard, Mike Sheetz, Julie Theriot, Tim Mitcheson and John Condeelis.

Appendices

A. A molecular picture of gel osmotic pressure

The conventional thermodynamic and statistical mechanical descriptions of osmotic pressure are completely adequate for describing equilibrium situations. However, in the spirit of the molecular dynamics models we employ here it may be enlightening to some readers to give an alternate picture of gel osmotic pressure. A more complete description can be found in [34].

Consider the polyelectrolyte gel shown in Figure A1a. The fixed charges on the gel restrict the mobile counterions to the confines of the gel—almost. Those whose diffusion carries them beyond the gel boundary experience a strong electric field pulling them back. Indeed, the repulsive electric double layer acts like a semipermeable membrane for the counterions, and so the counterions can be viewed as a solute ‘gas’ confined to the gel. These solutes particles are driven by three forces: the random forces produced by collisions with the water molecules, the frictional force between the water and the particles, and the repulsive force of the membrane⁵. Let $\mathbf{X}_k(t)$ be the position of the k th particle; then the motion can be described by a Langevin equation of the form:

$$m \frac{d^2 \mathbf{X}_k}{dt^2} = - \underbrace{\left(\mathbf{X}_k \right)}_{\text{External force on particle } k} + \underbrace{\bar{\mathbf{u}}(\mathbf{X}_k(t), t) - \frac{d\mathbf{X}_k}{dt}}_{\text{Frictional force between particle } k \text{ and fluid with velocity } \bar{\mathbf{u}}} + \underbrace{\mathbf{R}_k(t)}_{\text{Random force exerted on particle } k \text{ by the fluid}} \quad [\text{A1}]$$

Here, the term $-\nabla$ represents all of the forces on the k th particle, including the effects of neighboring particles and the repulsive potential of the electrostatic membrane. \mathbf{R} is the random force, and $\bar{\mathbf{u}}$ is the *average* velocity of the water in the vicinity of the particle: $\bar{\mathbf{u}}(\mathbf{X}_k, t) = \int \mathbf{u}(\mathbf{x}, t) \phi_a(\mathbf{x} - \mathbf{X}_k) d\mathbf{x}$, where ϕ_a is a weighting function. The motion of the fluid can be described by the Navier-Stokes equations:

⁵ Note that the frictional force between the fluid and the particle also arises from the random impacts of water molecules on the particle.

$$\frac{\mathbf{u}}{t} + \mathbf{u} \cdot \mathbf{u} + p = \mu \nabla^2 \mathbf{u} - \underbrace{\sum_{k=1}^N \int d(\mathbf{x} - \mathbf{X}_k(t)) \bar{\mathbf{u}}(\mathbf{X}_k(t), t) - \frac{d\mathbf{X}_k}{dt}}_{\text{Frictional and random forces exerted on the fluid by the particles}} + \mathbf{R}_k(t) \quad [\text{A2}]$$

This is simply Newton's second law: the forces the fluid exerts on the particles is the negative of the force the particles exert on the fluid. The key feature here is the last term which couples the motion of the particles with the fluid motion. That is, the viscous drag force exerted by the fluid on each particle is felt equally by the fluid, but in the opposite direction. Also, the random force acting on the particles arises from the statistical fluctuations in the fluid near the particle, and so the same force must act reciprocally on the fluid volume surrounding the particle. If this force were applied at a point, it would produce an infinite velocity there. Instead, we spread the force out over a fluid volume of diameter λ by making use of the weighting function $\int d(\mathbf{x} - \mathbf{X}_k)$. Once we have decided to spread the force in this way, conservation of energy demands that we also average the fluid velocity using the same weighting function. Since we are interested in motions on a cellular scale, we can neglect inertial terms in these equations, and insist that the fluid be incompressible: $\nabla \cdot \mathbf{u} = 0$.

For motions on cellular scales fluid inertia is negligible, and equation [A2] becomes

$$\nabla^2 \mathbf{u} = \frac{1}{\mu} \nabla p + \sum_{k=1}^N \int d(\mathbf{x} - \mathbf{X}_k(t)) [- \mathbf{F}_k] \quad [\text{A3}]$$

This says that the fluid motion, \mathbf{u} , is driven by the hydrostatic pressure gradient augmented by the force exerted on the fluid at the interface: the forces, $-\mathbf{F}_k$, felt by the particles are now transferred to the fluid as an additional force term. Notice that the only randomness in the fluid equations is the location of the particles.⁶ The equilibrium case, $\mathbf{u} = 0$, is enlightening:

⁶ It may appear strange that the frictional coupling coefficient, μ , doesn't appear in Equation [8]. Note, however, that Equation [8] must be solved simultaneously with Equation [6] for the particle locations, $\mathbf{X}_k(t)$, and the fluid velocity field, $\mathbf{u}(\mathbf{x}, t)$. The limiting situation where $\mu \rightarrow 0$ is singular: with no drag, the particles move at infinite velocity, and so neglect of the particle mass is not possible. For any finite particle drag, all

$$p = - \sum_{k=1}^N \frac{d}{d\mathbf{x}} (\mathbf{x} - \mathbf{X}_k) \cdot \mathbf{X}_k \quad [\text{A4}]$$

If we assume that the particles do not interact, take an ensemble average of these two equations and then integrate them across the membrane, we obtain van't Hoff's law of osmotic pressure: $p = RT \cdot c$, where c is the molar concentration of the solute particles [34].

The picture of osmotic pressure that emerges from this model is shown in Figure A1b. According to Equation [A1] particles diffusing close to the gel boundary have their random motions biased away from the boundary by the electrostatic force $-\nabla \phi$, and this force exerted on the particles is transferred to the fluid via viscous drag. The electrostatic membrane and the particles repel one another causing the particles to drag fluid away from the membrane. Seen from this viewpoint, *osmotic pressure is generated by biasing the Brownian motion of the solute particles*, which induces a directional viscous drag of the fluid by the particles. In a conventional membrane equilibrium, the particles would drag more fluid away from the membrane than towards it until an opposing pressure head is built up that just counters the aggregate drag of the solutes. This is the osmotic pressure. In an immersed gel, however, the fluid is incompressible and so the fluid drag by the solutes (counterions and gel fibers) simply builds up the hydrostatic pressure within the gel. The fibers of the gel diffuse outward because of their entropic writhing, and in the absence of counterions, their motion is described adequately by a diffusion equation (c.f. equation B2 below). The presence of counterions adds a surface force to this diffusion: by pushing inwards on the counterions, the electrostatic membrane drags the gel fibers at the surface outward (since it is electrically coupled to them). Therefore, a swelling ionic gel has a surface force that augments its entropic swelling.

B. Swelling of a polyelectrolyte gel

The stress tensor characterizing the cortical actin cytogel has the form: $\sigma = \sigma_{\text{elastic}} + \sigma_{\text{osmotic}}$, where the elastic stresses are due to the (entropic and bending) elasticity of the actin fibers,

of the force, \mathbf{f}_k , on the particle is transmitted to the fluid, and so the fluid equations do not contain \mathbf{f}_k .

and the osmotic pressure arises from the entropic motions of the fibers and the counterion pressure. The balance between viscous, elastic and osmotic forces leads to the swelling equation:

$$\frac{\mathbf{u}}{t} = \sigma, \quad [\text{B1}]$$

where $\mathbf{u}(r,t)$ is the radial displacement field from the final (swollen) state, and σ is the friction coefficient between the gel fibers and the cytosol. Tanaka et al. [24, 44] assumed that the elastic stress is linear and isotropic, and neglected the ion pressure contribution to the osmotic pressure. Then, for spherical swelling where shear deformations are small, they showed that the swelling equation takes the form of a linear diffusion equation in u :

$$\frac{u}{t} = \hat{D}^2 u \quad [\text{B2}]$$

with diffusion coefficient $\hat{D} = (K + 4\mu/3)/\eta$, where K and μ are the bulk and shear modulus of the gel, respectively. With a stress-free boundary condition, $\sigma_{rr} = 0$, this results in a time course for swelling governed by the time constant $\tau \sim R^2 / \hat{D} = R^2 \eta / E$, where R is the final radius of the swollen gel, and E is the elastic modulus of the gel. E and η were considered constant, although for large swelling ratios they would be expected to vary.

An ionic gel follows a different time course because the ion pressure contributes an additional nonlinear, radial stress [12, 38]. Therefore, an exact expression for large swelling of ionic gels is still lacking. However, from the theory of osmotic pressure in Appendix A [34] we see that the mechanical swelling equation is coupled to the diffusion of counterions at the gel-solvent interface:

$$\frac{c}{t} = D_c \nabla^2 c - [\mu F_E(u) \delta(r - R) c] \quad [\text{B3}]$$

where $c(r,t)$ is the concentration of counterions in the electrical double layer at the gel surface $r = R(t)$, $\mu = D_c/k_B T$ their mobility coefficient, F_E is the electrical force coupling the counterions to the gel macroions, and $\delta(r - R(t))$ is a unit vector normal to the gel surface. The restraining force exerted on the boundary counterions by the gel acts reciprocally on the gel surface, so the swelling equation becomes

$$\frac{u}{t} = \hat{D}^{-2} u + F_E(u(R)) \quad [\text{B4}]$$

i.e. the diffusion of the gel fibers is augmented by the outward directed surface pressure exerted by the counterions in the double layer. The exact form of $F_E(\cdot)$ is complicated, but it should be proportional to the concentration of the macroion charge density at the gel surface, $c_p(R)$. If $D_c \gg \hat{D}$ (i.e. the ions reach their equilibrium distribution faster than the gel diffuses), then $F_E = c(R) \cdot c_p(R)$; this varies $\propto c^2$, in agreement with the usual expression for the osmotic pressure of a polyelectrolyte gel derived from Donnan equilibrium [38]. The initial swelling rate is governed by the linearization of [B3], which has the form $\frac{c}{x} = D_c \frac{c^2}{x^2} - \text{const.} \times c$, i.e. the counterion diffusion is retarded by its electrical coupling to the outer surface of the gel. This retarding force on the ions is felt by the gel surface as an expansive force, and so a term $\propto c$ must be added to the swelling equation. Since $c \propto 1/\text{gel volume}$, the gel should expand initially as:

$$\frac{dR}{dt} = E(R_0 - R) + \frac{A}{R^n} \quad [\text{B5}]$$

where $E(\cdot) = (K + 4\mu/3)/R_0$ is the elastic modulus for the gel which, via K and μ , is proportional to the crosslink density, ν . The constant A contains the chain concentration, the degree of ionization of the polymer and the ionic strength of the solvent, and the exponent, $n \geq 1$ depends on the geometry. The time constant for the initial swelling is $1/E \sim \text{Lim}_{t \rightarrow 0} (dR/dt) = \nu \cdot \tau_{\text{neutral}}$, where $\nu < 1$ and τ_{neutral} is the relaxation time of the gel if it were neutral. Thus a polyelectrolyte gel far from its isoelectric (uncharged) pI always swells faster than the corresponding neutral gel. Note that equation [B5] implies that the initial swelling of a spherical bleb ($n = 2$) should follow $d(\text{volume})/dt = \text{constant}$.

C. The speed of a Brownian Ratchet

We model a polymerizing actin filament as a linear array of monomers; here, the ratchet mechanism is the intercalation of monomers between the barrier and the polymer tip, as shown in Figure 3a. Denote the gap width between the tip of the rod and the barrier by g , and the size of a monomer by a . When a sufficiently large fluctuation occurs the gap opens wide enough to allow a monomer to polymerize onto the end of the rod. The polymeriza-

tion rate is given by $R = k_{\text{on}}(\cdot) \cdot M -$, where M is the local monomer concentration and the polymerization rate constant; $k_{\text{on}}(\cdot) \cdot M$, reflects the *conditional* probability of adding a monomer when the gap width is \cdot . We set $k_{\text{on}}(\cdot) \cdot M =$ when $\cdot >$, and $k_{\text{on}}(\cdot) \cdot M = 0$ when $\cdot <$. We can obtain a formula for the velocity of the BR by writing a diffusion equation for the density of particles $c(\cdot, t)$, where \cdot is the gap width [36]:

$$\frac{c}{t} = D \frac{\partial^2 c}{\partial x^2} + \frac{fD}{k_B T} \frac{\partial c}{\partial x} + [c(x + \cdot, t) - H(\cdot - x)c(x, t)] + [H(\cdot - x)c(x - \cdot, t) - c(x, t)] \quad (\text{C1})$$

Here D is the diffusion coefficient of the load, $-f$ is the load force (i.e. to the left, opposing the motion), $H(\cdot - x)$ is the Heaviside step function ($= 0$ for $\cdot < x$, and $= 1$ for $\cdot > x$). The boundary conditions are that $\partial c / \partial x = 0$ is reflecting and $c(\cdot, t)$ is continuous at $\cdot = x$. The steady state solution to equation (1b) gives the force-velocity relation if we define the ratchet velocity by $v(\cdot) = \int_0^\cdot \alpha(x) dx - \int_0^\cdot \beta(x) dx$ (i.e. we weight the polymerization velocity by the probability of a \cdot -sized gap). When depolymerization can be neglected, i.e. $k_{\text{off}} \ll$ —which is the case for actin polymerization—we obtain:

$$v = \frac{2D}{\mu} \frac{(\mu - \frac{f}{k_B T})^2}{\mu^2 + (e^{-\mu} - 1)\mu}, \quad (\text{C2})$$

where μ is the dimensionless work done against the load: $\mu = f \cdot / k_B T$, and $\mu(\cdot, \cdot, D) >$

is given by solving the transcendental equation, $\frac{2}{D} \frac{1 - e^{-\mu}}{\mu} + \mu - = 0$. If the polymerization and depolymerization velocities are much slower than the ideal ratchet velocity, i.e. $\cdot, \cdot \ll 2D/$, then the ratchet equation can be solved explicitly for $\cdot > 0$ to yield equation (1b).

NOTE: Another approach to the ratchet problem is to solve for the mean first passage time for a particle to traverse the interval $(0, \cdot)$. This involves solving the following diffusion equation:

$$D \frac{\partial^2 T}{\partial x^2} + \frac{Df}{k_B T} \frac{\partial T}{\partial x} = -1$$

subject to the boundary conditions:

$$\text{Reflecting at } x = 0: \frac{T(0)}{x} = 0, \quad \text{Partially reflecting at } x = l: -D \frac{T(l)}{x} = v T(l)$$

where v is the polymerization velocity. The result is:

$$v = \frac{D^2}{D(e^{-1}) + (e^{-1} - 1)}$$

Although the formula looks somewhat different, the load velocity curve is practically the same.

BIBLIOGRAPHY

1. Alt, W. Models of cytoplasmic motion (1988). *From Chemical to Biological Organization*. Marcus, Miller and Nicolis ed. Springer-Verlag. New York.
2. Argiro, V., M. Bunge and M. Johnson (1985). A quantitative study of growth cone filopodial extension. *J. Neurosci. Res.* **13**: 149-62.
3. Bo, L. and R. E. Waugh (1989). Determination of bilayer membrane bending stiffness by tether formation from giant, thin-walled vesicles. *Biophys. J.* **55**(3): 509-517.
4. Bray, D., N. Money, F. Harold and J. Bamberg (1991). Responses of growth cones to changes in osmolality of the surrounding medium. *J. Cell Sci.* **98**(4): 507-515.
5. Cunningham, C. C., T. P. Stossel and D. J. Kwiatkowski (1991). Enhanced Motility in NIH 3T3 Fibroblasts That Overexpress Gelsolin. *Science.* **251**: 1233-1236.
6. Dabiri, G. A., J. M. Sanger, D. A. Portnoy and F. S. Southwick (1990). *Listeria monocytogenes* moves rapidly through the host-cell cytoplasm by inducing directional actin assembly. *Proc. Natl. Acad. Sci. (USA).* **87**(16): 6068-6072.
7. Dembo, M. (1986). The mechanics of motility in dissociated cytoplasm. *Biophys. J.* **50**: 1165-1183.
8. Dembo, M. (1989). Mechanics and Control of the Cytoskeleton in *Amoeba proteus*. *Biophys. J.* **55**: 1053-1080.
9. Dembo, M. and F. Harlow (1985). Cell motion, contractile networks, and the physics of interpenetrating reactive flow. **50**: 109-121.
10. Evans, E. and A. Yeung (1989). Apparent viscosity and cortical tension of blood granulocytes determined by micropipet aspiration. *Biophys. J.* **56**(1): 151-60.
11. Felder, S. and E. L. Elson (1990). Mechanics of fibroblast locomotion: quantitative analysis of forces and motions at the leading lamellas of fibroblasts. *J. Cell Biol.* **111**: 2513-2526.
12. Flory, P. J. (1989). *Statistical Mechanics of Chain Molecules*. ed. Oxford University Press. New York.
13. Forscher, P., C. H. Lin and C. Thompson (1992). Inductopodia: A novel form of stimulus-evoked growth cone motility involving site directed actin filament assembly. *Nature.* **357**(6378): 515-518.
14. Hartwig, J. and M. DeSisto (1991). The cytoskeleton of the resting human blood platelet: Structure of the membrane skeleton and its attachment to actin filaments. *J. Cell Biol.* **112**(3): 407-425.

15. Hartwig, J. J. Shevlin (1986). The architecture of actin filaments and the ultrastructural location of actin-binding protein in the periphery of lung macrophages. *J. Cell Biol.* **103**:1007-1020.
16. Jacobson, A., G. Odell and G. Oster. The cortical tractor model for epithelial folding: application to the neural plate (1985). *Molecular Determinants of Animal Form*. Edelman ed. Alan R. Liss. New York.
17. Jacobson, A., G. Oster, G. Odell and L. Cheng (1986). Neurulation and the cortical tractor model for epithelial folding. *J. Embryol. exp. Morphol.* **96**: 19-49.
18. Janmey, P., C. Cunningham, G. Oster and T. Stossel. Cytoskeletal networks and osmotic pressure in relation to cell structure and motility (1992). *Swelling Mechanics: From Clays to Living Cells and Tissues*. Karalis ed. Springer-Verlag. Heidelberg.
19. Janmey, P. A. and T. P. Stossel (1989). Gelsolin-Polyphosphoinositide Interaction. **264**: 4825-4831.
20. Kucik, D. F., E. L. Elson and M. P. Sheetz (1989). Forward Transport of Glycoproteins on Leading Lamellipodia in Locomoting Cells. **340**: 315-317.
21. Landau, L. and E. Lifshitz (1970) . *The Theory of Elasticity*. ed. Pergamon. London.
22. Mitchison, T. and M. Kirschner (1984). Dynamic instability of microtubule growth. *Nature*. **312**: 237-42.
23. Nanavati, C. and J. M. Fernandez (1993). The secretory granule matrix: a fast-acting smart polymer. *Science*. **259**: 963-965.
24. Nossal, R. (1988). On the elasticity of cytoskeletal networks. *Biophys. J.* **53**: 349-59.
25. Odell, G. Amoeboid motions (1977). *Modern Modeling of Continuum Phenomena. Lectures in Applied Mathematics*. Amer. Math. Soc. Providence, RI.
26. Odell, G. (1977). A continuum theory of Allen's frontal contraction model of amoeboid pseudopodium extension. *J. Mechanochem. Cell Motility*. **4**: 1-13.
27. Odell, G. and J. Bonner (1986). How the *Dictyostelium discoideum* grex crawls. *Phil. Trans. R, Soc. Lond. B.* **312**: 487-525.
28. Oster, G. Mechanics of Cytogels (1984). *Modelling of Patterns in Space and Time*. W. Jager ed. Springer-Verlag. Berlin.
29. Oster, G. (1988). Biophysics of the leading lamella. *Cell Motil. Cytoskel.* **10**: 164-171.

30. Oster, G. Cell motility and tissue morphogenesis (1989). *Cell Shape: Determinants, Regulation and Regulatory Control*. Stein and Bronner ed. Academic Press. New York.
31. Oster, G. and G. Odell (1984). The mechanochemistry of cytogels. *Physica*. **12D**: 333-350.
32. Oster, G. and A. Perelson. The physics of cell motility. (1988). *J. Cell Sci. Suppl.: Cell Behavior: Shape, Adhesion and Motility*. J. Heaysman ed.
33. Oster, G., A. Perelson and L. Tilney (1982). A mechanical model for acrosomal extension in *Thyone*. *J. Math. Biol.* **15**: 259-65.
34. Oster, G. and C. Peskin. Dynamics of osmotic fluid flow (1992). *Mechanics of Swelling: From Clays to Living Cells and Tissues*. Karalis ed. Springer-Verlag. New York.
35. Perelson, A. S. and E. A. Coutsias (1986). A moving boundary model of acrosomal elongation. *J. Math. Biol.* **23**: 361-79.
36. Peskin, C., G. Odell and G. Oster (1993). Cellular motions and thermal fluctuations: The Brownian ratchet. *Biophys. J.* (In press):
37. Pollard, T. (1986). Rate constants for the reactions of ATP- and ADP-actin with the ends of actin filaments. *J. Cell Biol.* **103**(6): 2747-2754.
38. Richards, E. G. (1980) . *An Introduction to Physical Properties of Large Molecules in Solution*. ed. Cambridge University Press. New York.
39. Sanger, J. M., J. W. Sanger and F. S. Southwick (1992). Host cell actin assembly is necessary and likely to provide the propulsive force for intracellular movement of *Listeria monocytogenes*. *Infection & Immunity*. **60**(9.): 3609-3619.
40. Sheetz, M. P., D. B. Wayne and A. L. Pearlman (1992). Extension of filopodia by motor-dependent actin assembly. *Cell Motil. Cytoskel.* **22**(3): 160-169.
41. Stossel, T. (1990). How cells crawl. *Amer. Sci.* **78**: 408-23.
42. Theriot, J. and T. Mitchison (1992). Comparison of actin and cell surface dynamics in motile fibroblasts. *J. Cell Biol.* **118**(2): 367-377.
43. Theriot, J. and T. Mitchison (1992). The nucleation-release model of actin filament dynamics in cell motility. *Trends in Cell Biology*. **2**(8): 219-222.
44. Theriot, J. A., T. J. Mitchison, L. G. Tilney and D. A. Portnoy (1992). The rate of actin-based motility of intracellular *Listeria monocytogenes* equals the rate of actin polymerization. *Nature*. **357**: 257-60.
45. Tilney, L. and S. Inoue (1985). Acrosomal reaction of the Thyone sperm. III. The relationship between actin assembly and water influx during the extension of the acrosomal process. *J. Cell Biol.* **100**: 1273-83.

46. Tilney, L. G. and D. A. Portnoy (1989). Actin filaments and the growth, movement, and spread of the intracellular bacterial parasite, *Listeria monocytogenes*. *J Cell Biol.* : 1597-1608.
47. Trinkaus, J. (1984) . *Cells into Organs: Forces that Shape the Embryo. (2nd Ed.)*. ed. Prentice Hall. Englewood Cliffs, NJ.
48. Yin, H. and T. Stossel. Calcium control of actin network structure by gelsolin. (1982). *Calcium and Cell Function*.
49. Yonemura, S. and T. D. Pollard (1992). The localization of myosin I and myosin II in *Acanthamoeba* by fluorescence microscopy. *J Cell Sci.* : 629-42.

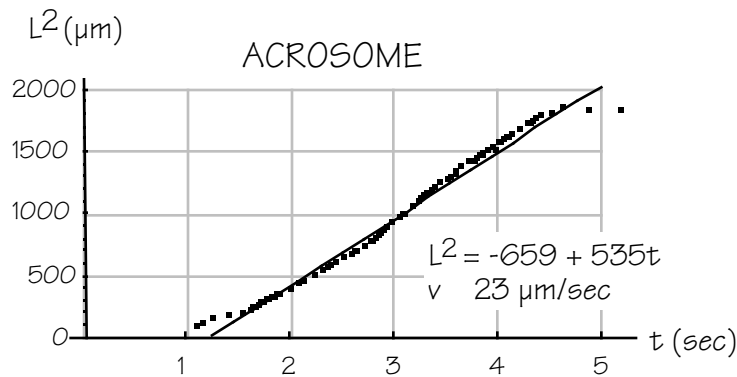
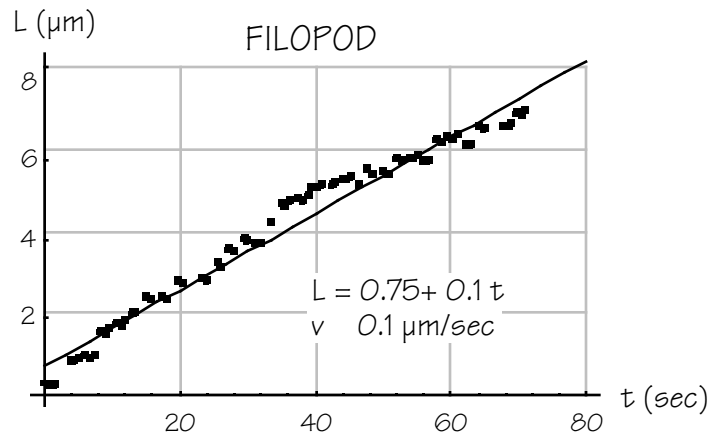
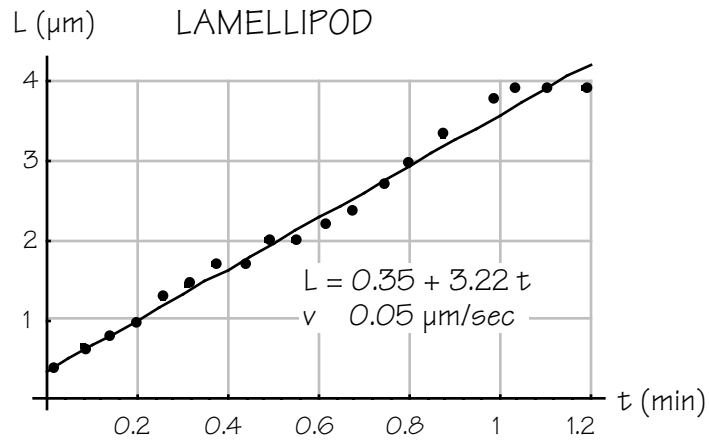


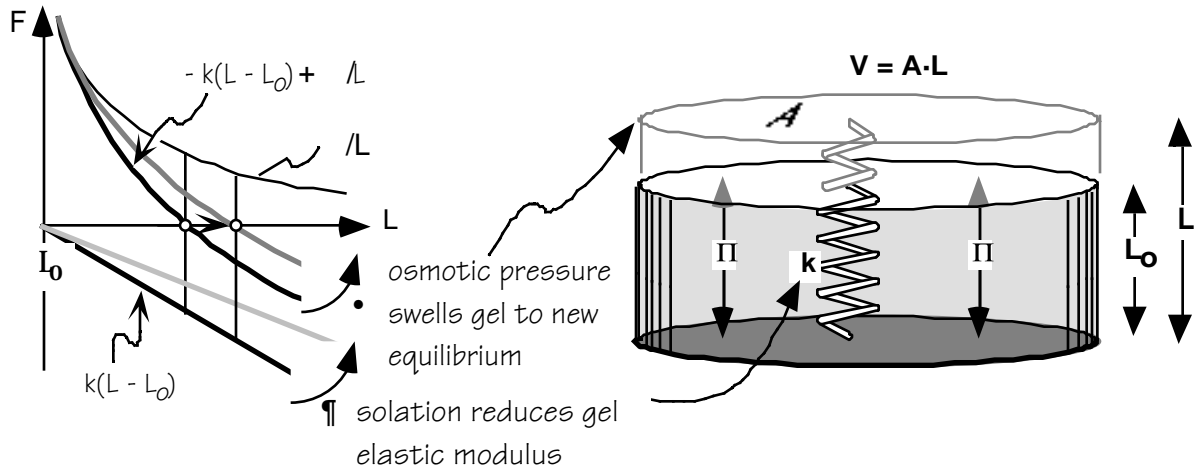
Figure 1. Extension velocities of three types of cellular protrusions.

Top: lamellipod, $v \sim 0.05 \mu\text{m}/\text{sec}$.

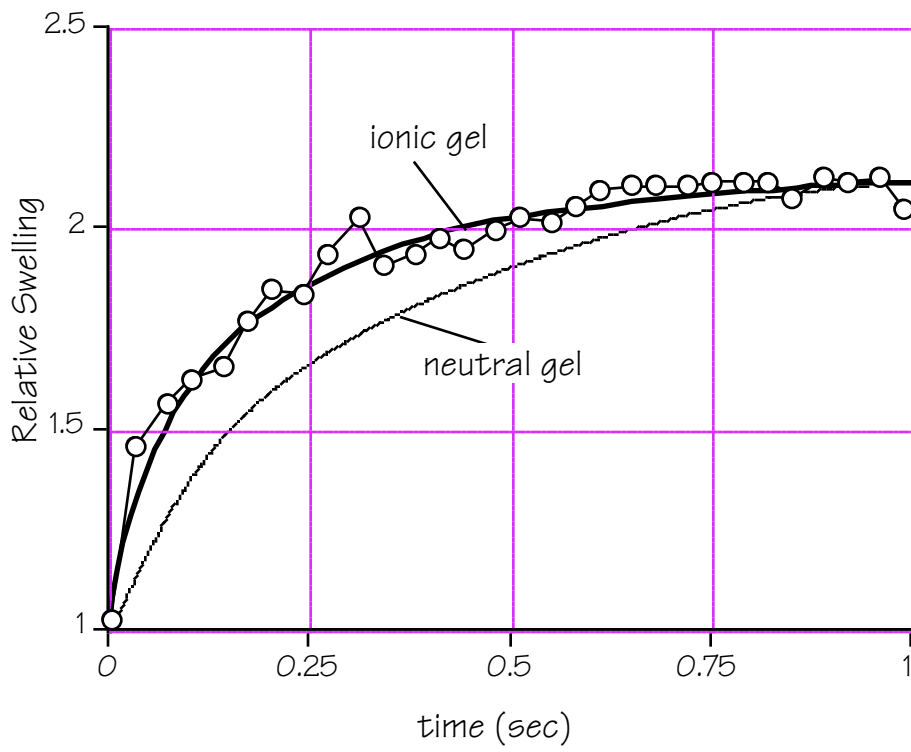
Middle: filopod, $v \sim 0.1 \mu\text{m}/\text{sec}$

Lower: acrosomal process in *Thyone*, $v \sim 23 \mu\text{m}/\text{sec}$

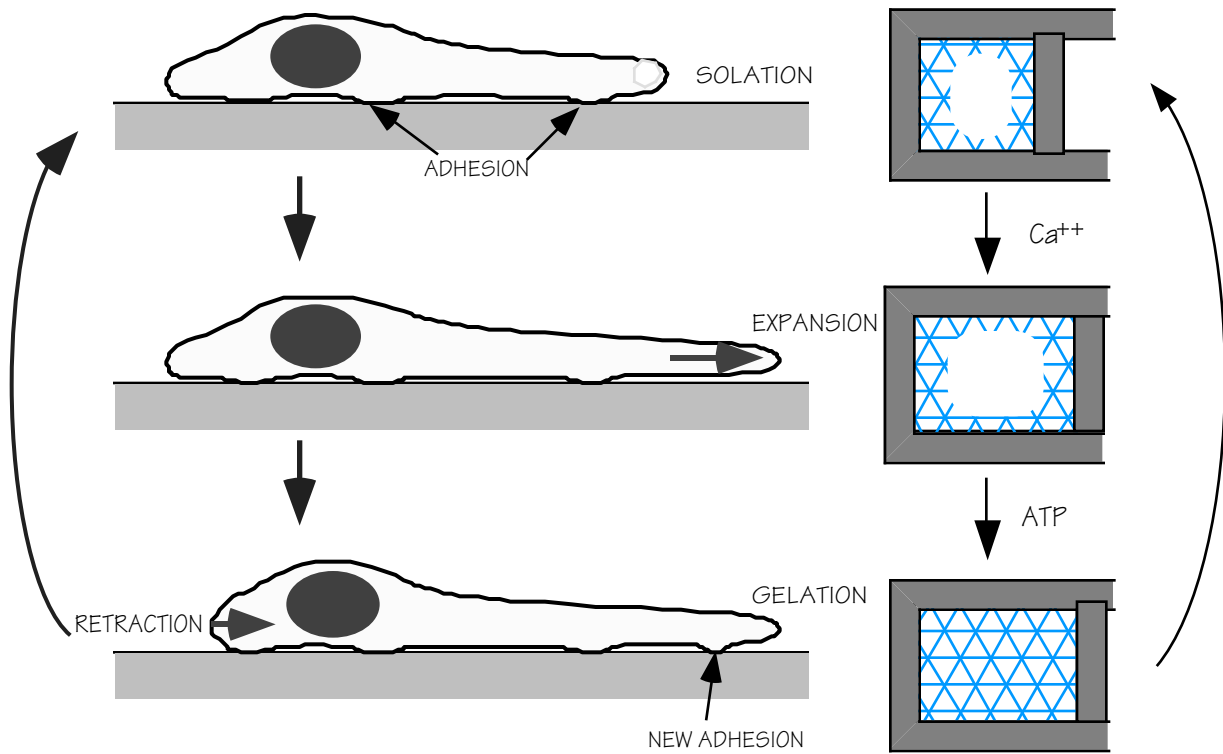
Velocities were obtained from a linear least-squares fit to the data. That these velocities differ by an order of magnitude or more suggests that they may be driven by different physical mechanisms.



(a)



(b)

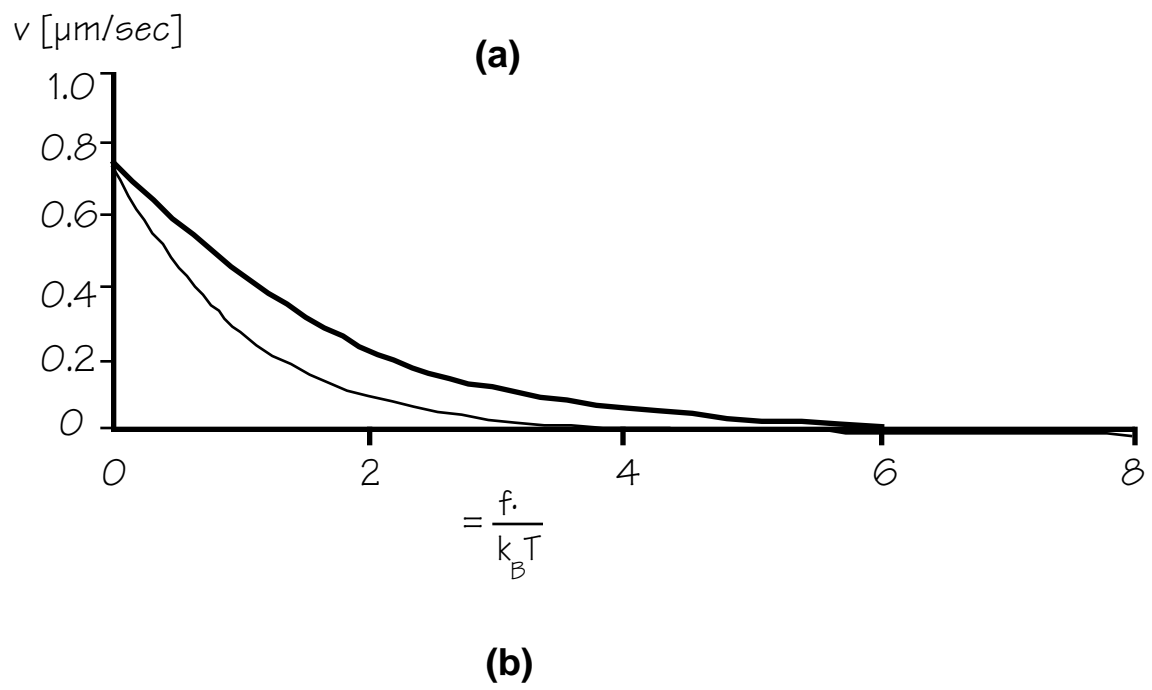
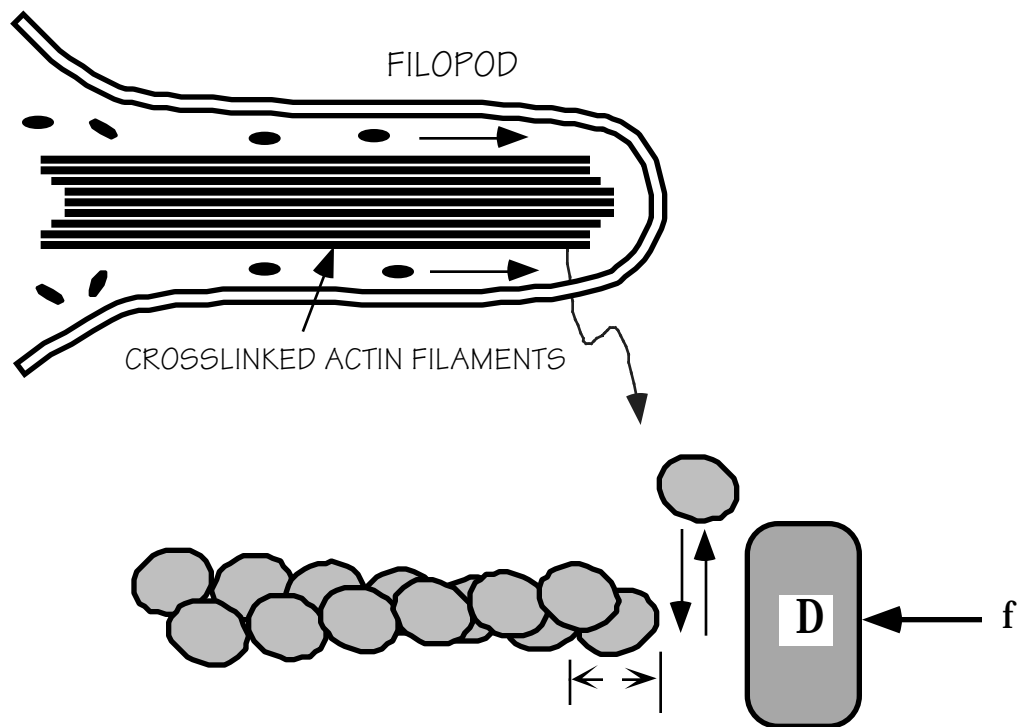


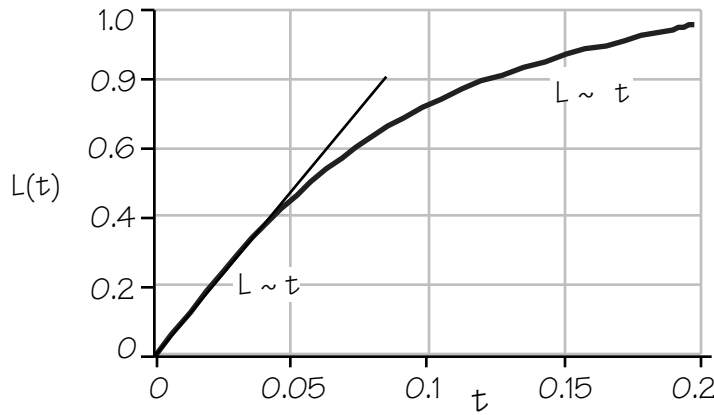
(c)

Figure 2. (a) A piece of cytogel is in mechanical equilibrium when the osmotic pressure, P , just balances the elastic restoring forces of the fibers. The forces in piece of actin cytogel can be visualized schematically as an opposition between the swelling pressure, P_s , due principally to the mobile counterions, and the restraining elastic forces exerted by the gel fibers. The elasticity of the gel is represented by a collection of springs with spring constant k , which is proportional to the number of chains, or cross-links, in the gel. When the gel is solated, the elastic modulus decreases: $k \rightarrow k - k_c$, and the gel swells to a new equilibrium.

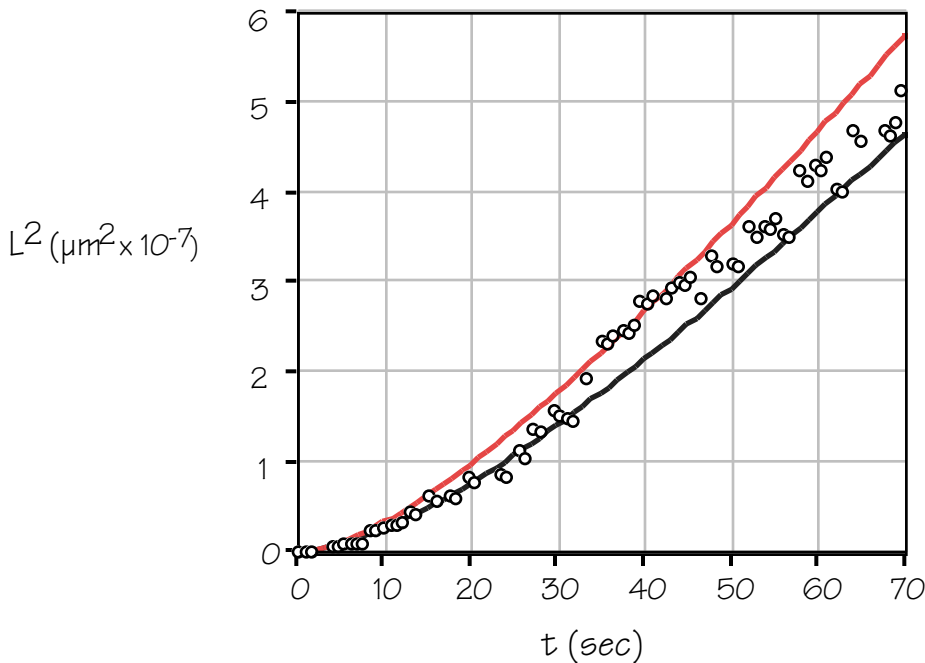
(b) The swelling of a biopolymer gel. The matrix from a mast cell granule (a negatively charged heparin sulfate proteoglycan) was subjected to a step in voltage at $t = 0$. This initiates swelling whose time course is fit well by the equation for an ionic gel. The neutral gel equation swells much more slowly in the early stages, but both approach nearly the same final swelling ratio. (Data from [26]).

(c) The solation-expansion cycle driving lamellipodial protrusion. Solation factors (e.g. gelsolin) sever some of the actin fibers thus reducing the elastic modulus of the gel. The osmotic pressure then swells the gel towards a new mechanical equilibrium. Finally, the gel reanneals as the actin repolymerizes and crosslinks. ATP hydrolysis drives the cycle via its facilitation of actin polymerization.





(c)



(d)

Figure 3. (a) The filopod has a core of actin filaments that polymerize at the tip. There are about 20 filaments (only one of which is shown here) with a polymerization rate $\dot{L} = k_{on}M - k_{off}$

$$\dot{L} = k_{on}M - k_{off}$$

(b) The load-velocity curve for a Brownian ratchet. The solid line is equation [A2], which applies for $k_{off} \sim 0$, and the dotted line is the approximate equation [1] which applies when

$\dot{L} \ll k_{on}M$ and $\dot{L} \ll k_{off} \ll 2D/\lambda$. For a filopod working against a membrane tension of 0.035

dyne/cm, $\lambda \sim 7.24$. (c) Filopodial protrusion rate begins as $L \sim t$, then decreases to $L \sim \sqrt{t}$ as the shaft grows so long that diffusion of monomers from the base limits polymerization at the tip.

(d) Solution to equations (2a) and (2b) compared to the data of Argiro, et al. (1985).

Parameter values were: $k_{on} = 11.3 / \mu\text{M}\cdot\text{sec}$, $k_{off} = 1.4/\text{sec}$, $n = 25 = 2.12 \times 10^3 \mu\text{M}$, $\lambda =$

$2.5 \times 10^{-7} \text{ cm}$, radius = 50 nm, $\lambda = 1.5$, $D_M = 5 \times 10^{-7} \text{ cm}^2/\text{sec}$, $L_0 = 5 \times 10^{-6} \mu\text{m}$. The data are

bracketed by the two curves for cytoplasmic monomer concentrations of $M_0 = 30 \mu\text{M}$ (bottom) and $35 \mu\text{M}$ (top).

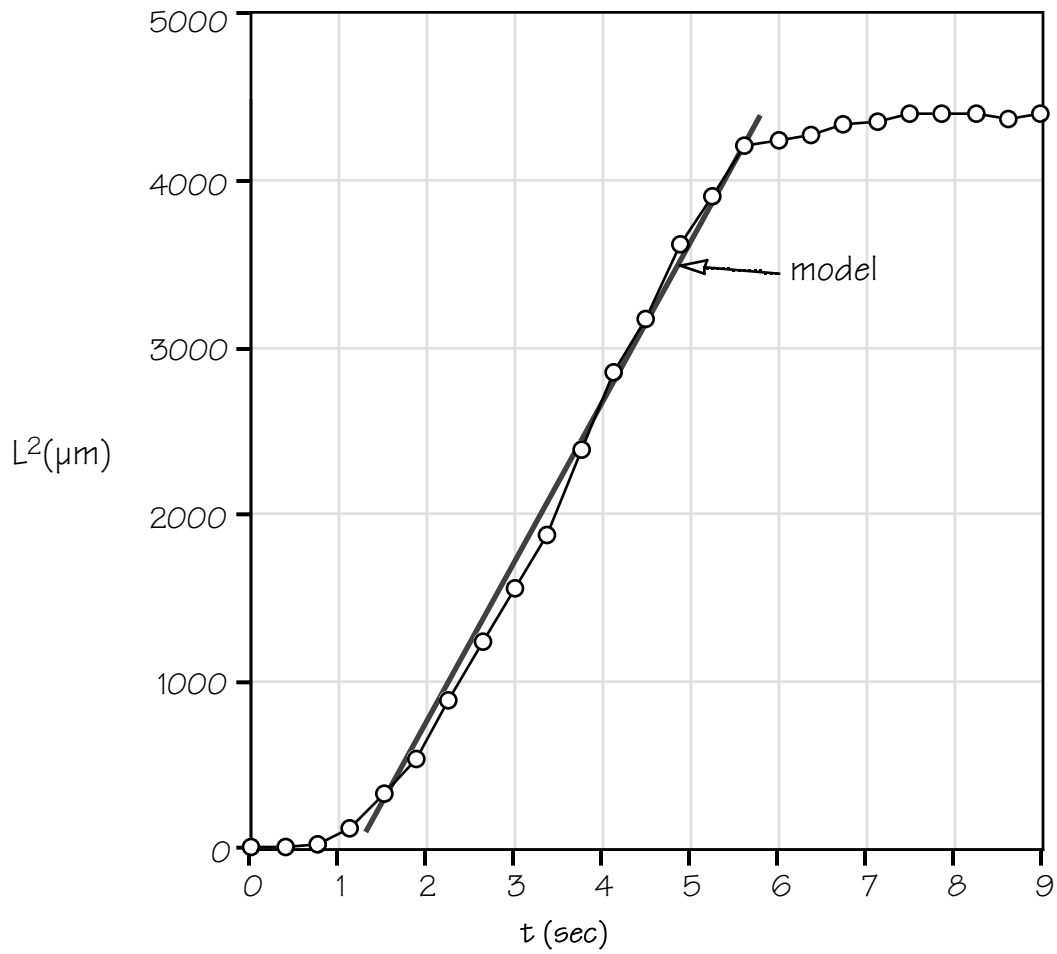
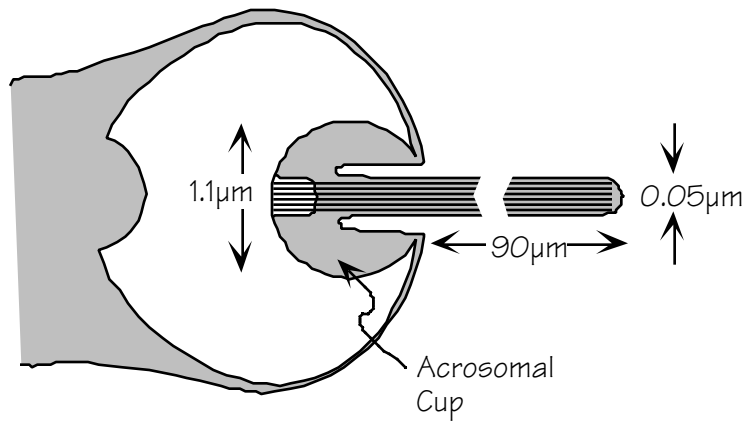


Figure 4. The acrosome of *Thyone* projects nearly 90 μm in less than 9 seconds. During most of its trajectory it follows a $L \sim t$ law. The circles are data from (3) and the solid line is the hydrostatic-osmotic model (20, 47).

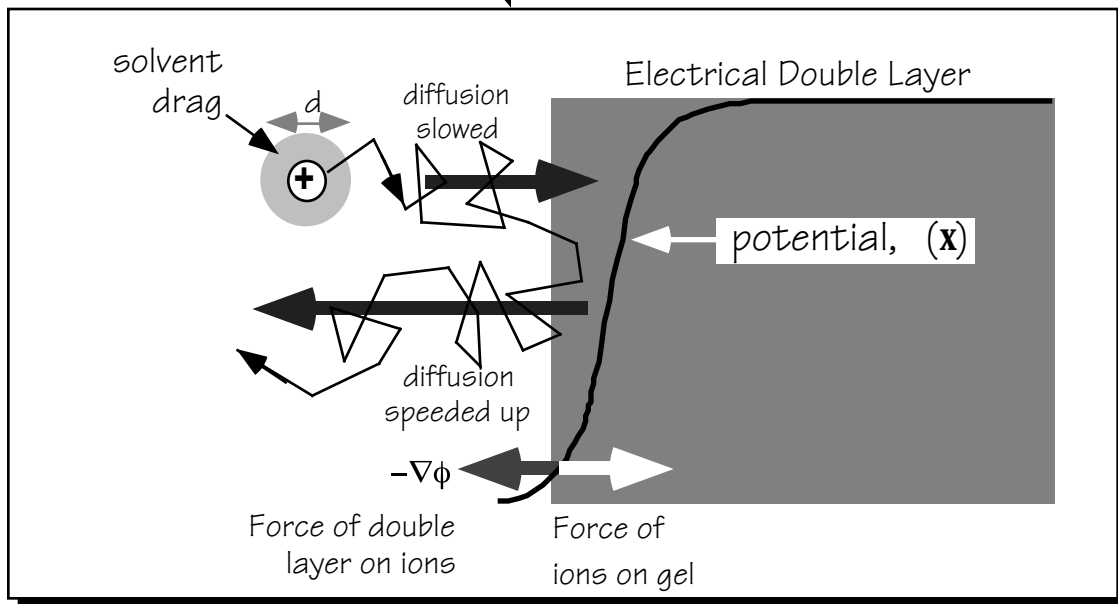
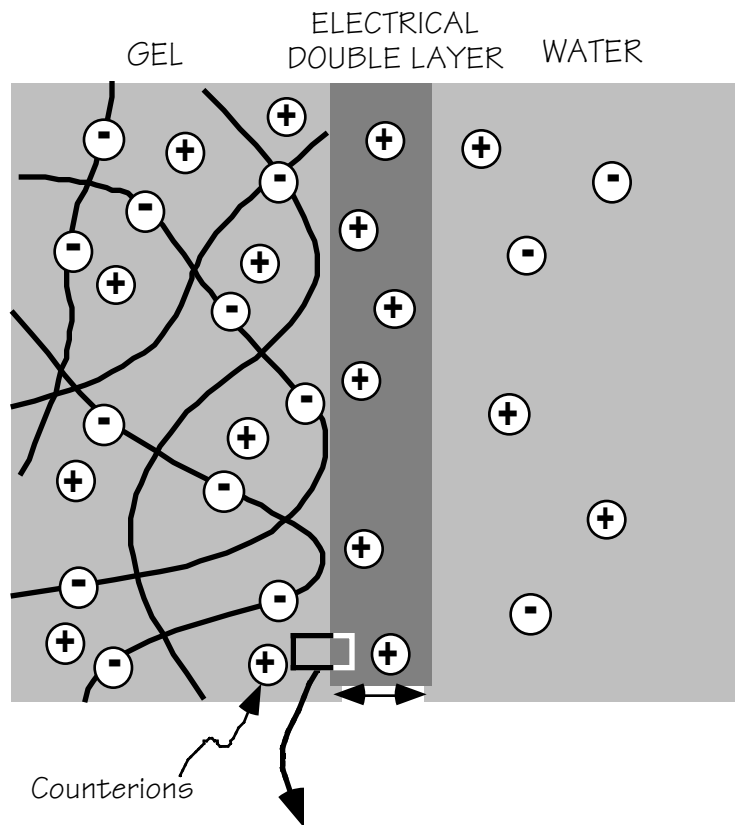


Figure. A1. The surface region of a polyelectrolyte gel. The fixed charges on the gel attract counterions so that the concentration of mobile solutes within the gel region exceeds that of the outside solvent. These excess cations cannot escape the gel because of the strong electrical field set up at the interface. A counterion approaching the interface from the inside is repelled back into the gel interior. Thus the double layer applies a force, $-$, to the solvent via the viscous drag each ion exerts on the solvent in a region d , and conversely, the diffusing counterions exert a pull on the fibers of gel surface as they try and escape down their concentration gradient.